

Uniturbulence and Alfvén wave solar model

T. Van Doorselaere¹, M. V. Sieyra², N. Magyar¹, M. Goossens¹, and Luka Banović¹

¹ Centre for mathematical Plasma Astrophysics, Department of Mathematics, KU Leuven, Celestijnenlaan 200B, B-3001 Leuven, Belgium

e-mail: tom.vandoorselaere@kuleuven.be

² Département d'Astrophysique/AIM, CEA/IRFU, CNRS/INSU, Université Paris-Saclay, Université de Paris, F-91191, Gif-sur-Yvette, France

Received ; accepted

ABSTRACT

Context. AWSOM-type models (van der Holst et al. 2014) have been very successful in describing the solar atmosphere by incorporating the Alfvén wave driving as extra contributions in the global MHD equations. However, they lack the contributions from other wave modes.

Aims. In this paper, we aim to write governing equations for the energy evolution equation of kink waves. In a similar manner as AWSOM, we combine the kink wave evolution equation with MHD. Our goal is to incorporate the extra heating provided by the uniturbulent damping of the kink waves. We attempt to construct the UAWSOM equations (uniturbulence and Alfvén wave driven solar models).

Methods. We have recently described the MHD equations in terms of the Q -variables. These latter variables allow to follow the evolution of waves in a co-propagating reference frame. We transform the Q -variable MHD equations into an energy evolution equation. First we do this generally, and then we specialise to the description of kink waves. We model the resulting UAWSOM system of differential equations in a 1D solar atmosphere configuration in a python code. We also couple this evolution equation to the slowly varying MHD formulation and solve the system in 1D.

Results. We find that the kink wave energy evolution equation contains non-linear terms, even in the absence of counterpropagating waves. Thus, we confirm earlier analytical and numerical results. The non-linear damping is expressed solely through equilibrium parameters, rather than an ad-hoc perpendicular correlation term (popularly quantified with a length scale L_{\perp}), as in the case of the AWSOM models. We have combined the kink evolution equation with the MHD equations to obtain the UAWSOM equations. A proof-of-concept numerical implementation in python shows that the kink wave driving indeed leads to radial outflow and heating. Thus, UAWSOM may have the necessary ingredients to drive the solar wind and heat the solar corona against losses.

Conclusions. Not only does our current work constitute a pathway to fix shortcomings in heating and wind driving in the popular AWSOM model, it also provides the mathematical formalism to incorporate more wave modes (e.g. the parametric decay instability) for additional driving of the solar wind.

Key words. Magnetohydrodynamics (MHD) – Plasmas – Waves – Methods: analytical – Methods: numerical – Sun: oscillations

1. Introduction

There are observational indications that the solar corona and the solar wind are filled with Alfvén waves. In-situ observations allow us to measure Alfvén waves directly in the solar wind (Bruno & Carbone 2013). However, in the corona they are usually only identified as spectral line broadenings. From spectroscopic measurements, it was thought that the Alfvén waves' energy is considerable (Banerjee et al. 1998; Hahn & Savin 2013; Pant & Van Doorselaere 2020). Only recently, a few direct measurements have become available (De Pontieu et al. 2012; Shetye et al. 2021; Petrova et al. 2024). As such, the true energy content of Alfvén waves in the corona is not so well established.

On the other hand, high-resolution imaging observations from SDO/AIA and SolO/EUI have shown clearly that loops and plumes show ubiquitous transverse motions (Anfinogentov et al. 2013; Nakariakov et al. 2024). Since the loop is displaced from its axis, these transverse motions are often identified as kink waves (Van Doorselaere et al. 2008; Goossens et al. 2009), in contrast to Alfvén waves which are thought to have a torsional motion in a cylindrical structure. The transverse waves manifest as the decayless transverse waves (Tian et al. 2012; Wang et al. 2012; Nisticò et al. 2013) in coronal loops. These loops are thought to be steadily fed with energy from its convective footpoint motions (e.g. Karampelas & Van Doorselaere 2021, and references therein) in order to counteract the strong damping that is observed for impulsively excited waves during flares (e.g. Nechaeva et al. 2019, and references therein). They have a standing character (Anfinogentov et al. 2015), even though that is not so clear in very short loops (Gao et al. 2022; Shrivastav et al. 2023).

In coronal plumes or long coronal loops, the transverse waves are observed as propagating waves (Tomczyk & McIntosh 2009; Thurgood et al. 2014). Also these propagating waves are found to be damped (Tiwari et al. 2021), although the weak damping rate seems to suggest only low density contrasts (Morton et al. 2021). It is unclear how these propagating kink waves are transformed

higher up to Alfvén waves (as they should, as evidenced in PSP observations, see e.g. Parashar et al. 2020) when the density contrast of the plumes is vanishing.

All these transverse waves must carry a significant amount of Poynting energy flux to the higher layers of the solar atmosphere. Energy estimates from observations go from a few W/m^2 (Tomczyk et al. 2007; Thurgood et al. 2014) to several 1000W/m^2 (Petrova et al. 2023). While some of the individual observed oscillations could counteract the heating requirements of quiet Sun or even active regions, the potential of wave heating with transverse waves was only recently studied in a statistical way. Lim et al. (2023) have performed a meta-analysis of transverse wave events reported in the literature to show that their energy forms a power law of their frequency, with a supercritical slope. Thus, Lim et al. (2023) found that transverse waves can heat the corona when acting as an ensemble.

All these observational results motivated the development of 3D heating models for coronal loops and plumes (Van Doorselaere et al. 2020b). These models rely on the development of resonant absorption (e.g. Goossens et al. 1992) kickstarting the Kelvin-Helmholtz instability (Terradas et al. 2008; Antolin & Van Doorselaere 2019). The KHI further develops under continued driving and encompasses the whole loop (Karampelas & Van Doorselaere 2018). In some simulations, this mechanism was able to balance the losses by optically thin radiative losses (Shi et al. 2021), although that seems to be strongly dependent on the specific loop’s conditions (De Moortel & Howson 2022). Moreover, the heating provided by propagating transverse waves has been modeled in a section of the corona by Magyar & Nakariakov (2021), and similar models for coronal heating by Alfvén waves have been constructed by Suzuki & Inutsuka (2005); Shoda et al. (2019) and follow-up works. Despite the promise that these numerical models hold, it has as yet not been possible to model the entire solar atmosphere heated with these wave heating mechanisms, because of the required numerical resources. So, it is necessary and instructive to parametrise the heating by transverse waves as 1D wave heating models and apply it to the full solar atmosphere. One example of this parametrisation is shown by Verdini et al. (2010), who incorporate turbulent heating from Alfvén waves and are able to explain the heating of plasma in a expanding coronal hole and the acceleration of the solar wind.

More recently, other models driven by Alfvén waves have been developed in 3D (AWSOM by van der Holst et al. 2014; Downs et al. 2016; Réville et al. 2020). Such models are being used all over the world for space weather forecasting. They are excellent at predicting the overall shape of the solar corona (Riley et al. 2019). Nowadays, similar models are being used to model stellar atmospheres as well (see e.g. Alvarado-Gómez et al. 2022; Evensberget & Vidotto 2024; Cohen et al. 2024, for some recent references). However, in these models, only the wave driving power of the Alfvén waves is taken into account. Moreover, the influence of background plasma structuring, except the structuring of the waves themselves (see L_{\perp}), perpendicular to the magnetic field on the wave dynamics has been ignored, despite efforts from Evans et al. (2012). Here, we are motivated by the observations to also incorporate kink wave driving of the solar and stellar atmospheres, following the approaches taken for the modelling of Alfvén wave driving.

To accomplish this, we use the recent description for wave dynamics in terms of Q -variables (Van Doorselaere et al. 2024). These Q -variables allow to track single waves in a co-propagating manner, and to include non-linear effects. The latter turns out to be important for propagating kink waves, because they are known to show a turbulent evolution for a single wave pulse (Magyar et al. 2017). This phenomenon has been named “uniturbulence”, because contrary to Alfvén wave turbulence in a uniform background, only one unidirectional kink wave is needed to generate small scales. This has been explained by Magyar et al. (2019); Van Doorselaere et al. (2020a) by showing that kink waves naturally consist of both Elsässer variables simultaneously, which are constantly interacting. That leads to damping of surface Alfvén waves in numerical simulations and analytical theory (Ismayilli et al. 2022).

Van Doorselaere et al. (2024) have provided the mathematical framework of the Q -variables and have rewritten the MHD equations in that formalism. We have shown in that paper that the Q -variables allow a general wave perturbation to be split in its constituent wave modes. This would thus allow us to complement the AWSOM idea (i.e. the MHD equations for the large scale evolution of the corona, complemented with Alfvén wave evolution equations) with an additional equation for the kink wave evolution.

In this paper, we first generalise the kink wave description to a flowing plasma as in the solar wind in Sec. 2. Then we recapitulate the MHD equations in terms of Q -variables (as found in Van Doorselaere et al. 2024) in Sec. 3. From the combination of these sections, we derive a general energy evolution equation in the Q -formalism in Sec. 4.1. Then we specialise this equation to the propagation and damping of kink waves (Sec. 4.1.3. Eventually, we formulate the set of equations for MHD plus Alfvén and kink evolution equations in Sec. 5, which we call the UAWSOM (uniturbulence and Alfvén wave solar models) equations. Finally, we present the initial results of a proof-of-concept implementation in a python package (Sec. 6).

2. Kink wave variables and terminology

For the UAWSOM model, we consider the additional driving of kink waves in flux tubes, next to the Alfvén waves. We consider the solar atmosphere filled with flux tubes, aligned with the magnetic field. The flux tubes we consider ought to model the coronal plumes which carry the main magnetic wave energy out into the solar wind. As such, in this section we first need to extend the model of Van Doorselaere et al. (2020a) to also include the background flow. However, since many of the calculations are identical to the equations and steps in Van Doorselaere et al. (2020a), we only keep the bare minimum needed to get the required expressions for the calculations in Sec. A.

To model kink waves in coronal plumes with background flow, we take an equilibrium configuration of a straight cylinder with homogeneous magnetic field $\mathbf{B}_0 = B_0 \mathbf{e}_z$ and constant and uniform background flow of $\mathbf{V} = V \mathbf{e}_z$, without gravity, and no gas pressure $p = 0$. In the first instance, we consider these equilibrium quantities not (or only weakly) to vary with height. We will relax this assumption in later sections, in a WKB-way. Our current configuration is most easily described by the cylindrical coordinate system

(r, φ, z) . We take a radial step function in density

$$\rho_0(r) = \begin{cases} \rho_i & \text{for } r \leq R, \\ \rho_e & \text{for } r > R. \end{cases}$$

The subscripts i, e are associated with the interior and exterior region respectively. R here is the radius of the coronal plume.

As in Van Doorselaere et al. (2020a), we take the total pressure perturbation $P' = \frac{B_0 \delta B_z}{\mu}$ as basic variable. We only consider propagating waves in this paper, which we describe with

$$P'(r, \varphi, z, t) = \mathcal{R}(r) \cos \varphi \cos(k_z z - \omega t). \quad (1)$$

The function $\mathcal{R}(r)$ has the radial dependence of the pressure variation, for which we use the thin-tube limit $\delta = k_z R \ll 1$, and write

$$\mathcal{R}(r) = \begin{cases} A \frac{r}{R} & \text{for } r \leq R \\ A \frac{R}{r} & \text{for } r > R, \end{cases} \quad (2)$$

with wave amplitude A . According to Goossens et al. (1992), in the thin-tube limit for a uniform flow, the wave frequency equals the kink frequency

$$\omega = k_z V \pm \omega_k, \quad \text{with} \quad \omega_k = \sqrt{\frac{2k_z^2 B_0^2}{\mu(\rho_i + \rho_e)}} = \omega_{Ae} \sqrt{\frac{2}{\zeta + 1}}, \quad (3)$$

and where we have introduced the Alfvén frequency $\omega_A = k_z V_A$ (in connection with the Alfvén speed $V_A = \mathbf{B}_0 / \sqrt{\mu \rho}$, with magnetic permeability μ) and the density contrast of the coronal plume as $\zeta = \rho_i / \rho_e > 1$, which we take to be greater than 1 always.

We compute the velocity components (v_r, v_φ, v_z) using Eq. 10-11-12 of Goossens et al. (1992):

$$\delta V_r = \frac{1}{\rho_0(\Omega^2 - \omega_A^2)} \frac{\partial}{\partial r} \frac{dP'}{dt}, \quad \delta V_\varphi = \frac{1}{\rho_0(\Omega^2 - \omega_A^2)} \frac{1}{r} \frac{\partial}{\partial \varphi} \frac{dP'}{dt}, \quad \delta V_z = 0, \quad (4)$$

where the latter statement is true because of the cold plasma limit. In these equations, the total derivative $d/dt = \partial/\partial t + V\partial/\partial z$ is the Lagrangian derivative. Moreover, $\Omega = \omega - k_z V$ is the Doppler-shifted frequency. The expression for the total derivative is also the reason why we only consider propagating waves here (in contrast to Van Doorselaere et al. 2020a): for standing waves, the time derivative and z -derivative result in a change of $z - t$ behaviour in both terms for standing waves.

With these notations, we can also relate the amplitude A of the total pressure variations with the amplitude Υ of the velocity perturbations generalising what we have obtained in Van Doorselaere et al. (2020a):

$$\Upsilon = \frac{A}{R} \frac{\Omega}{\rho_0(\Omega^2 - \omega_A^2)}, \quad (5)$$

where we now include the effect of background flow.

In what follows, we will also need the expressions for the magnetic field perturbation $\delta \mathbf{B}$. For the remainder of this paper, we will consider $\delta B_z = 0$, because Van Doorselaere et al. (2020a) have shown that its contributions are always higher order in $k_z R$ (even though we took $P' = B_0 \delta B_z / \mu \neq 0$ before!). For the other magnetic field components, we linearise the induction equation ($\partial \mathbf{B}_0 / \partial t = \nabla \times (\mathbf{V} \times \mathbf{B}_0)$) for a flowing plasma. The result for the components perpendicular to the magnetic field is

$$\frac{\partial \delta \mathbf{B}_\perp}{\partial t} = B_0 \frac{\partial}{\partial z} \delta \mathbf{V}_\perp - V \frac{\partial}{\partial z} \delta \mathbf{B}_\perp - \delta \mathbf{B}_\perp \nabla \cdot \mathbf{V}. \quad (6)$$

In the last term, we left the dependence on the divergence of \mathbf{V} . In this cylindrical system, it is of course 0, but in the full model later on, it will be non-zero. Still, we leave this term out here, because it is smaller (in a WKB sense) than the wave variations in the first two terms on the RHS.

In the end, we generalise the expressions from Van Doorselaere et al. (2020a) for the velocity and magnetic field perturbations, and we find that the generalisation is limited to replacing ω by the Doppler-shifted frequency Ω :

$$\delta V_r = \frac{\partial \mathcal{R}}{\partial r} \frac{\Omega}{\rho_0(\Omega^2 - \omega_A^2)} \cos \varphi \sin(k_z z - \omega t), \quad (7)$$

$$\delta V_\varphi = -\frac{\mathcal{R}}{r} \frac{\Omega}{\rho_0(\Omega^2 - \omega_A^2)} \sin \varphi \sin(k_z z - \omega t), \quad (8)$$

$$\delta B_r = -\frac{\partial \mathcal{R}}{\partial r} \frac{k_z B_0}{\rho_0(\Omega^2 - \omega_A^2)} \cos \varphi \sin(k_z z - \omega t), \quad (9)$$

$$\delta B_\varphi = \frac{\mathcal{R}}{r} \frac{k_z B_0}{\rho_0(\Omega^2 - \omega_A^2)} \sin \varphi \sin(k_z z - \omega t), \quad (10)$$

$$\delta B_z = 0. \quad (11)$$

In Van Doorselaere et al. (2020a) (and corresponding to the expression in Goossens et al. 2013), we had computed with these variables (in a setting without flow) that the wave energy density is given as

$$\langle w \rangle = \pi R^2 \frac{\rho_i + \rho_e}{2} \Upsilon^2, \quad (12)$$

which is averaged over the cross-section and the wavelength. Here, the wave energy w is given as

$$w^\pm = \frac{\rho_0 (\delta \mathbf{Z}^\pm)^2}{4}, \quad (13)$$

and

$$\delta \mathbf{Z}^\pm = \delta \mathbf{V} \pm \frac{\delta \mathbf{B}}{\sqrt{\mu \rho_0}} \quad (14)$$

is the linearised version of the classical Elsässer variable $\mathbf{Z} = \mathbf{V} \pm V_A$. We then compute w by

$$w = w^+ + w^-. \quad (15)$$

We sum both of these to cover the entirety of the wave energy, because the kink wave has both Elsässer components non-zero (Magyar et al. 2019; Van Doorselaere et al. 2020a).

For the wave pressure P_k , Van Doorselaere et al. (2020a) found

$$P_{ki} = \frac{\omega_{Ai}^2}{2\rho_i(\Omega^2 - \omega_{Ai}^2)^2} \left(\frac{A}{R}\right)^2 \sin^2(k_z z - \omega t), \quad (16)$$

$$P_{ke} = \frac{\omega_{Ae}^2}{2\rho_e(\Omega^2 - \omega_{Ae}^2)^2} \left[\frac{A^2 R^2}{r^4}\right] \sin^2(k_z z - \omega t), \quad (17)$$

which we generalised immediately to have the Doppler-shifted frequency Ω instead.

From these generalisations of the kink wave functions of Van Doorselaere et al. (2020a) to plumes that now include background flow, it seems that the influence of the flow is limited to replacing the wave frequency ω with the Doppler-shifted frequency Ω in all expressions.

3. Q -variables and terminology

A second ingredient that is needed to formulate the UAWSOM model are the Q -variables. These were introduced in Van Doorselaere et al. (2024) as variables that are co-propagating variables with the waves's phase speeds. They are defined as

$$\mathbf{Q}^\pm = \mathbf{V} \pm \alpha \mathbf{B}, \quad (18)$$

where α is a parameter related to the phase speed of the wave. In Van Doorselaere et al. (2024) we have shown that these Q -variables are well suited to track any wave. Thus, we will use them to construct extra equations for propagating kink waves in plume regions, on top of the existing Alfvén waves equations in the AWSOM model. Constructing these extra equations is possible, because Q -variables have as extra property that waves propagating in one direction only have non-zero components in the co-propagating Q -component, generalising the convenience of the Elsässer variables for Alfvén waves to all other waves. We briefly list in this section the necessary notation and equations that form the basis for constructing the energy evolution equation for kink waves in coronal plumes.

In our previous work Van Doorselaere et al. (2024), we have shown that the MHD equations are rewritten in terms of Q -variables, with the following form of the momentum and induction equation

$$\begin{aligned} \frac{D^\mp}{Dt} \mathbf{Q}^\pm \mp \left(\frac{\mathbf{Q}^+ - \mathbf{Q}^-}{4}\right) \frac{D^\mp}{Dt} \ln \rho \alpha^2 = & -v_s^2 \nabla \ln \rho - \frac{1}{8} \left(1 - \frac{\Delta \alpha^2}{\alpha^2}\right) \nabla (\mathbf{Q}^+ - \mathbf{Q}^-)^2 + \frac{1}{4} \left(1 - \frac{\Delta \alpha^2}{\alpha^2}\right) (\mathbf{Q}^+ - \mathbf{Q}^-)^2 \nabla \ln \alpha \\ & - \frac{1}{4} \frac{\Delta \alpha^2}{\alpha^2} (\mathbf{Q}^+ - \mathbf{Q}^-) \cdot \nabla (\mathbf{Q}^+ - \mathbf{Q}^-) + \frac{1}{4} \frac{\Delta \alpha^2}{\alpha^2} (\mathbf{Q}^+ - \mathbf{Q}^-) \nabla \cdot (\mathbf{Q}^+ - \mathbf{Q}^-) \\ & \mp \left(\frac{\mathbf{Q}^+ - \mathbf{Q}^-}{8}\right) \nabla \cdot (3\mathbf{Q}^\pm - \mathbf{Q}^\mp) + \left(\frac{\mathbf{Q}^+ - \mathbf{Q}^-}{4}\right) \left(\left(\frac{\mathbf{Q}^+ - \mathbf{Q}^-}{2}\right) \cdot \nabla \ln \rho \alpha^2\right). \end{aligned} \quad (19)$$

In this equation, we have employed the notation for the co-moving derivative $\frac{D^\pm}{Dt} = \frac{\partial}{\partial t} + \mathbf{Q}^\pm \cdot \nabla$, the parameter $\Delta \alpha^2 = \alpha^2 - \frac{1}{\mu \rho}$ measures the deviation of the wave from an Alfvén wave, and $v_s^2 = \frac{\gamma p}{\rho}$ is the square of the sound speed for a plasma with pressure p . Using the expression for the continuity relation

$$\frac{D^\pm}{Dt} (\ln \rho) = -\frac{1}{2} \nabla \cdot (3\mathbf{Q}^\pm - \mathbf{Q}^\mp) \pm \frac{\mathbf{Q}^+ - \mathbf{Q}^-}{2} \cdot \nabla \ln \rho \alpha^2, \quad (20)$$

here we will use Eq. 19 in the form

$$\begin{aligned} \frac{D^\mp}{Dt} \mathbf{Q}^\pm \mp \left(\frac{\mathbf{Q}^+ - \mathbf{Q}^-}{4} \right) \frac{D^\mp}{Dt} \ln \rho \alpha^2 &= -v_s^2 \nabla \ln \rho - \frac{1}{8} \left(1 - \frac{\Delta \alpha^2}{\alpha^2} \right) \nabla (\mathbf{Q}^+ - \mathbf{Q}^-)^2 + \frac{1}{4} \left(1 - \frac{\Delta \alpha^2}{\alpha^2} \right) (\mathbf{Q}^+ - \mathbf{Q}^-)^2 \nabla \ln \alpha \\ &- \frac{1}{4} \frac{\Delta \alpha^2}{\alpha^2} (\mathbf{Q}^+ - \mathbf{Q}^-) \cdot \nabla (\mathbf{Q}^+ - \mathbf{Q}^-) + \frac{1}{4} \frac{\Delta \alpha^2}{\alpha^2} (\mathbf{Q}^+ - \mathbf{Q}^-) \nabla \cdot (\mathbf{Q}^+ - \mathbf{Q}^-) \\ &\mp \left(\frac{\mathbf{Q}^+ - \mathbf{Q}^-}{8} \right) \left(-2 \frac{D^\mp}{Dt} (\ln \rho) \pm (\mathbf{Q}^+ - \mathbf{Q}^-) \cdot \nabla \ln \rho \alpha^2 \right) + \left(\frac{\mathbf{Q}^+ - \mathbf{Q}^-}{4} \right) \left(\left(\frac{\mathbf{Q}^+ - \mathbf{Q}^-}{2} \right) \cdot \nabla \ln \rho \alpha^2 \right). \end{aligned} \quad (21)$$

For what follows, it is convenient to realise that

$$\mathbf{Q}^+ - \mathbf{Q}^- = 2\alpha \mathbf{B} \quad (22)$$

is in the direction of the magnetic field.

In our previous paper Van Doorselaere et al. (2024), we have used these equations to describe surface Alfvén waves. We have found that

$$\alpha = \alpha_L = \alpha_R = \sqrt{\frac{2}{\mu(\rho_R + \rho_L)}}, \quad (23)$$

which also helps to recover the kink frequency ω_k for such surface Alfvén waves. Given the correspondence between surface Alfvén waves and kink waves (especially in the long-wavelength limit, Goossens et al. 2012), we will utilise these α values for kink waves in cylinders (as in Sec. 2) as well. We have previously shown that such a choice of α allows to decouple and filter out the waves of interest, in casu the kink waves.

4. Wave energy equations

Now we can construct an energy evolution equation that will form the basis for the kink wave equation in the UAWSOM model. To that end, we start from the linearised Q -variable equations (Eq. 21) and transform it to an energy evolution equation.

We consider how the wave energy evolves in a system which has the magnetic field $\mathbf{B}_0(z)$, the density $\rho_0(z)$ and the wind velocity $\mathbf{V}(z)$ as functions of z and slowly evolving in time. The waves only have small perturbations on the background, and a classical linearisation of the system is suitable. This is not true higher up in the solar wind (say above $\sim 3 - 5$ solar radii), but (following van der Holst et al. 2014) we take this approximation nevertheless, because higher order (non-linear) terms are anyway included in the system. Thus, we consider

$$\mathbf{Q}^\pm = \mathbf{Q}_0^\pm + \delta \mathbf{Q}^\pm, \quad \text{and} \quad \ln \rho \approx \ln \rho_0 + \delta R, \quad \ln \rho \alpha^2 \approx \delta R + \ln \rho_0 \alpha^2, \quad (24)$$

where we have introduced the notation $\delta R = \delta \rho / \rho_0$. As in Van Doorselaere et al. (2024), the phase speed variable α is not linearised in this process. With the above linearisation, we obtain for the perpendicular components of $\delta \mathbf{Q}_\perp^\pm$:

$$\begin{aligned} \frac{D^\mp}{Dt} \delta \mathbf{Q}_\perp^\pm + \delta \mathbf{Q}_\perp^\mp \cdot \nabla \mathbf{Q}_0^\pm &= -v_s^2 \nabla \delta R \pm \frac{\alpha}{2} \delta \mathbf{B}_\perp \frac{D^\mp}{Dt} \ln \rho_0 \alpha^2 \pm \frac{\alpha}{2} \delta \mathbf{B}_\perp \frac{D^\mp}{Dt} \delta R - \Delta \alpha^2 \mathbf{B}_0 \cdot \nabla \delta \mathbf{B}_\perp - \Delta \alpha^2 \delta \mathbf{B}_\perp \cdot \nabla \delta \mathbf{B}_\perp \\ &- \frac{1}{\rho_0} \nabla P_w \mp \left(\frac{\delta \mathbf{Q}_\perp^+ - \delta \mathbf{Q}_\perp^-}{8} \right) \left[-2 \frac{D^\mp}{Dt} \ln \rho_0 - 2 \frac{D^\mp}{Dt} \delta R \pm (\delta \mathbf{Q}_\perp^+ - \delta \mathbf{Q}_\perp^-) \cdot \nabla \ln \rho_0 \alpha^2 \mp (\delta \mathbf{Q}_\perp^+ - \delta \mathbf{Q}_\perp^-) \cdot \nabla \delta R \right. \\ &\left. \pm (\mathbf{Q}_0^+ - \mathbf{Q}_0^-) \cdot \nabla \ln \rho_0 \alpha^2 \right] \\ &+ \left(\frac{\delta \mathbf{Q}_\perp^+ - \delta \mathbf{Q}_\perp^-}{8} \right) \left[(\mathbf{Q}_0^+ - \mathbf{Q}_0^-) \cdot \nabla \ln \rho_0 \alpha^2 + (\delta \mathbf{Q}_\perp^+ - \delta \mathbf{Q}_\perp^-) \cdot \nabla \ln \rho_0 \alpha^2 + (\delta \mathbf{Q}_\perp^+ - \delta \mathbf{Q}_\perp^-) \cdot \nabla \delta R \right], \end{aligned} \quad (25)$$

where we have conveniently left some terms in $\delta \mathbf{B}_\perp$ to shorten the notation. $P_w = \frac{\delta B^2}{2\mu}$ is the wave pressure in the equation. It will become either the kink wave pressure P_k or the Alfvén wave pressure P_A .

Because the kink wave is nearly incompressible, we take all terms with δR to be zero, since the kink wave's compression scales with $k_z^2 R^2$. Moreover, we assume that the perpendicular variations of equilibrium quantities (e.g. $\delta \mathbf{Q}_\perp^\mp \cdot \nabla \mathbf{Q}_0^\pm$) are also 0. This is in principle incorrect, because in the kink wave model of Sec. 2 large variations of density are present across the magnetic field. However, we will account for the effect of those gradients only through the use of α and averaging across the cross-section of the coronal plume. The resulting equation is then

$$\begin{aligned} \frac{D^\mp}{Dt} \delta \mathbf{Q}_\perp^\pm &= \pm \frac{\alpha}{2} \delta \mathbf{B}_\perp \frac{D^\mp}{Dt} \ln \rho_0 \alpha^2 - \Delta \alpha^2 \mathbf{B}_0 \cdot \nabla \delta \mathbf{B}_\perp - \Delta \alpha^2 \delta \mathbf{B}_\perp \cdot \nabla \delta \mathbf{B}_\perp \\ &- \frac{1}{\rho_0} \nabla P_w \mp \left(\frac{\delta \mathbf{Q}_\perp^+ - \delta \mathbf{Q}_\perp^-}{8} \right) \left[-2 \frac{D^\mp}{Dt} \ln \rho_0 \pm (\mathbf{Q}_0^+ - \mathbf{Q}_0^-) \cdot \nabla \ln \rho_0 \alpha^2 \right] + \left(\frac{\delta \mathbf{Q}_\perp^+ - \delta \mathbf{Q}_\perp^-}{8} \right) \left[(\mathbf{Q}_0^+ - \mathbf{Q}_0^-) \cdot \nabla \ln \rho_0 \alpha^2 \right]. \end{aligned} \quad (26)$$

It is sometimes convenient to take the limit of $\alpha^2 \rightarrow \frac{1}{\mu\rho}$, $\Delta\alpha^2 \rightarrow 0$, $\delta\mathbf{Q}_\perp^\pm \rightarrow \delta\mathbf{Z}^\pm$ to check the results. Here we can use this limit to see that the previous equation coincides in that limit with Eq. 20 of van der Holst et al. (2014). Since we have neglected perpendicular gradients of equilibrium quantities, we do not have their terms with gradients of \mathbf{u} and \mathbf{B} , but we did keep the term with the wave pressure.

The linear portion of the left term in Eq. 26 is

$$\frac{\partial}{\partial t} \delta\mathbf{Q}_\perp^\pm + \mathbf{Q}_0^\mp \cdot \nabla \delta\mathbf{Q}_\perp^\pm, \quad (27)$$

which shows that the wave propagates the speed $\mathbf{Q}_0^\mp = \mathbf{V} \mp \alpha\mathbf{B}_0$. This indicates at the same time that $\alpha\mathbf{B}_0$ is the phase speed of the wave, and also that $\delta\mathbf{Q}_\perp^\pm$ belongs to the downward propagating wave (if the magnetic field is pointing up).

4.1. Energy evolution

Following the procedure of van der Holst et al. (2014), we now multiply Eq. 26 with $\rho_0\delta\mathbf{Q}_\perp^\pm/2$. Then we have an evolution equation for the Q -density W^\pm :

$$W^\pm = \frac{\rho_0}{4} (\delta\mathbf{Q}_\perp^\pm)^2. \quad (28)$$

This expression is seemingly different than the wave energy density w (Eq. 13), but it is only an apparent difference. In appendix A, we show that

$$W^\pm = \rho_0 \delta V_\perp^2, \quad (29)$$

and thus that the Q -density is equal to the wave energy density w if the wave energy is in equipartition.

We will now use this Q -density to construct an energy evolution equation for the kink waves. As stated before, we multiply Eq. 26 with $\rho_0\delta\mathbf{Q}_\perp^\pm/2$. We then obtain

$$\frac{D^\mp}{Dt} W^\pm - W^\pm \frac{D^\mp}{Dt} \ln \rho_0 - \frac{1}{2} (W^\pm - CC) \frac{D^\pm}{Dt} \ln \rho_0 = -\Delta\alpha^2 \frac{\rho_0}{2} \delta\mathbf{Q}_\perp^\pm \cdot (\mathbf{B}_0 \cdot \nabla \delta\mathbf{B}_\perp) - \Delta\alpha^2 \frac{\rho_0}{2} \delta\mathbf{Q}_\perp^\pm (\delta\mathbf{B}_\perp \cdot \nabla \delta\mathbf{B}_\perp) + \frac{1}{2} (W^\pm - CC) \frac{D^\mp}{Dt} \ln \rho_0 \alpha^2, \quad (30)$$

where we have introduced the shorthand $CC = \rho_0 \frac{\delta\mathbf{Q}_\perp^+ \cdot \delta\mathbf{Q}_\perp^-}{4}$ for the cross-correlation between upward and downward propagating waves. We grouped the terms not involving $\Delta\alpha^2$ or $\ln \rho_0 \alpha^2$ (basically the effects of Alfvén waves, as was already incorporated in AWSOM) to the left-hand side. The term with the wave pressure was dropped at this stage, because (1) its net contribution is in the z -direction, and (2) the time and spatially averaged term is added to the momentum equation of the background (Eq. 59). In any case, the radial contribution of the pressure term has been averaged out previously.

We rewrite the left-hand side of the previous equation following the AWSOM lead of van der Holst et al. (2014), using the equation for the conservation of mass of the background plasma

$$\frac{\partial}{\partial t} \ln \rho_0 + \mathbf{V} \cdot \nabla \ln \rho_0 + \nabla \cdot \mathbf{V} = 0, \quad (31)$$

to obtain

$$\frac{D^\mp}{Dt} W^\pm - W^\pm \frac{D^\mp}{Dt} \ln \rho_0 - \frac{1}{2} (W^\pm - CC) \frac{D^\pm}{Dt} \ln \rho_0 = \frac{\partial W^\pm}{\partial t} + \nabla \cdot ((\mathbf{Q}_0^\mp + \delta\mathbf{Q}_\perp^\mp) W^\pm) + \frac{1}{2} CC \frac{D^\pm \ln \rho_0}{Dt} + W^\pm \left(\frac{1}{2} \nabla \cdot \mathbf{V} \pm \frac{1}{2} \alpha \mathbf{B}_0 \cdot \nabla \ln \rho_0 \alpha^2 \right), \quad (32)$$

where we have used once again the incompressibility of the wave mode and perpendicular gradients of background quantities to be zero. Finally, we obtain as evolution equation for the Q -density

$$\frac{\partial W^\pm}{\partial t} + \nabla \cdot ((\mathbf{Q}_0^\mp + \delta\mathbf{Q}_\perp^\mp) W^\pm) + \frac{1}{2} CC \frac{D^\pm \ln \rho_0}{Dt} + \frac{W^\pm}{2} \nabla \cdot \mathbf{V} = \frac{W^\pm}{2} \left(\frac{D^\mp}{Dt} \mp \alpha \mathbf{B}_0 \cdot \nabla \right) \ln \rho_0 \alpha^2 - \frac{CC}{2} \frac{D^\mp}{Dt} \ln \rho_0 \alpha^2 - \Delta\alpha^2 \frac{\rho_0}{2} \delta\mathbf{Q}_\perp^\pm \cdot (\mathbf{B}_0 \cdot \nabla \delta\mathbf{B}_\perp) - \Delta\alpha^2 \frac{\rho_0}{2} \delta\mathbf{Q}_\perp^\pm \cdot (\delta\mathbf{B}_\perp \cdot \nabla \delta\mathbf{B}_\perp). \quad (33)$$

The second term in the right-hand side of this equation in principle groups with the third term on the left-hand side. However, this way of writing is more elegant, because these right-hand side terms describe how the wave energy density evolution is modified if $\alpha \neq 1/\sqrt{\mu\rho}$, i.e. a different wave is considered than an Alfvén wave.

The rightmost term in this equation describes the energy dissipation by uniturbulence. There is self-interaction of the wave (any wave!) if $\Delta\alpha^2 \neq 0$, leading to a cascade of energy in a turbulent way (Ismayilli et al. 2024).

4.1.1. Characterisation of the uniturbulence term

Let us further specialise these equations for single kink waves, i.e. only taking into account the effect of the kink waves on themselves. The terms with $\ln \rho_0 \alpha^2$ will cancel out, because the α for the kink wave (Eq. 23) shows that it is still proportional to the density (interior or external does not matter here). The only variation in that term would be due to spatial and temporal variations of the density contrast ζ , but we will take these to be 0 in this paper, assuming that the density contrast and filling factor remain constant in the entire domain. Later on, in Sec. 6, the parameter ζ will in fact change with height, but its change is very small indeed, so the approximation here is fine.

For working out the uniturbulence terms, we consider that there is only one of δQ_{\perp}^{\pm} , in order to have only the self-interaction (Magyar et al. 2019). Then we can use Eq. 22 to write that

$$\delta Q_{\perp}^{\pm} = \pm 2\alpha \delta \mathbf{B}_{\perp}. \quad (34)$$

With this equation, we can rewrite

$$-\Delta \alpha^2 \frac{\rho_0}{2} \delta Q_{\perp}^{\pm} (\delta \mathbf{B}_{\perp} \cdot \nabla \delta \mathbf{B}_{\perp}) = \mp \Delta \alpha^2 \mu \rho_0 \alpha \delta \mathbf{B}_{\perp} \cdot \nabla P_k. \quad (35)$$

In the exterior region of the plume, the latter expression reduces to

$$\mp \frac{1-\zeta}{1+\zeta} \alpha \delta \mathbf{B}_{\perp} \cdot \nabla P_k, \quad (36)$$

where we have used the expression for α from Eq. 23. Using Eq. 7-11 (or Eq. 40 & 44 in Van Doorselaere et al. 2020a), we have that $\delta \mathbf{B}_{\perp i} \cdot \nabla P_{ki} = 0$ up to leading orders of $k_z R$. The remaining contribution for uniturbulent damping is

$$\delta \mathbf{B}_{\perp e} \cdot \nabla P_{ke} = -2 \frac{A^3 R^3}{r^7} \frac{k_z B_0 \omega_{Ae}^2}{\rho_e^2 (\Omega^2 - \omega_{Ae}^2)^3} \cos \varphi \sin^3 (k_z z - \omega t). \quad (37)$$

For the radial averaging, we integrate from R to γR as for the energy (as we have also done in Goossens et al. 2013; Van Doorselaere et al. 2014, 2020a, see also the procedure in Sec. A for an example). For that integral we have

$$\int_R^{\gamma R} \frac{1}{r^7} r dr = \frac{1}{5R^5} \left(\frac{\gamma^5 - 1}{\gamma^5} \right) = \frac{1}{5R^5} (1 - f^{5/2}). \quad (38)$$

As was discussed in Van Doorselaere et al. (2020a), the expression Eq. 37 is an odd-powered periodic function in φ and time, and its average would result in 0. Thus, it makes sense to take the RMS average of this term to quantify the uniturbulent damping. The physical interpretation is that all small scales are cascaded to even smaller scales before they experience the inverse cascade in the second half of the period. From Van Doorselaere et al. (2020a), we know that the RMS average will yield a $\sqrt{\pi}$ from the integral over φ , and the RMS average over t yields a factor $\sqrt{5/16}$. We then obtain as result

$$-\frac{\zeta - 1}{\zeta + 1} \sqrt{\pi} \sqrt{\frac{5}{16}} \frac{2A^3}{5R^2} \frac{\alpha k_z B_0 \omega_{Ae}^2}{\rho_e^2 (\Omega^2 - \omega_{Ae}^2)^3} (1 - f^{5/2}), \quad (39)$$

where we have kept the minus sign only to extract energy from the equation. Further substituting the relevant expressions for Υ (Eq. 5), we then write

$$-\frac{\zeta - 1}{\zeta + 1} \sqrt{\frac{\pi}{20}} \alpha k_z B_0 R \frac{\rho_e \omega_{Ae}^2 \Upsilon^3}{\Omega^3} (1 - f^{5/2}), \quad (40)$$

which is further simplified with the expression for $\Omega = \alpha k_z B_0$ to

$$-\frac{\zeta - 1}{\zeta + 1} \sqrt{\frac{\pi}{20}} R \frac{\rho_e \omega_{Ae}^2 \Upsilon^3}{\Omega^2} (1 - f^{5/2}). \quad (41)$$

Here we use once again that $\Omega = \pm \alpha k_z B_0 = \pm \omega_{Ae} \sqrt{\frac{2}{\zeta + 1}}$ to further simplify to

$$-\frac{\zeta - 1}{4} \sqrt{\frac{\pi}{5}} R \rho_e \Upsilon^3 (1 - f^{5/2}). \quad (42)$$

This expression is equal to the damping rate found in Van Doorselaere et al. (2020a), confirming the earlier result with the use of the new Q -variables. For the implementation in a numerical code, it is most convenient to write this term as an expression of the cross-section and wavelength-averaged energy density $\langle W^{\pm} \rangle$ (see Van Doorselaere et al. 2014, 2020a, and Sec. A for more details):

$$\langle W^{\pm} \rangle = \frac{k_z}{2\pi} \int_z dz \int_{\varphi} d\varphi \int_0^{\gamma R} W^{\pm} r dr = \pi R^2 \Upsilon^2 \frac{\rho_i + \rho_e (1-f)}{2}, \quad (43)$$

to

$$-\langle W^{\pm} \rangle^{3/2} \frac{1}{\pi R^2} \frac{1}{\sqrt{\rho_e}} \sqrt{\frac{2}{5}} \frac{\zeta - 1}{2} \frac{1 - f^{5/2}}{(\zeta + 1 - f)^{3/2}}. \quad (44)$$

4.1.2. Characterisation of the $\mathbf{B}_0 \cdot \nabla \delta \mathbf{B}_\perp$ term

In the previous subsection, we have simplified the energy cascade term for the uniturbulence damping mechanism. We will now simplify the remaining, unknown terms in Eq. 33. To that end, we use Eq. 34 to simplify the term in Eq. 33 containing $\mathbf{B}_0 \cdot \nabla \delta \mathbf{B}_\perp$:

$$-\Delta \alpha^2 \frac{\rho_0}{2} \delta \mathbf{Q}_\perp^\pm \cdot (\mathbf{B}_0 \cdot \nabla \delta \mathbf{B}_\perp) = \mp \Delta \alpha^2 \frac{\rho_0}{2} 2\alpha \delta \mathbf{B}_\perp \cdot (\mathbf{B}_0 \cdot \nabla \delta \mathbf{B}_\perp) = \mp \Delta \alpha^2 \mu \rho_0 \alpha \mathbf{B}_0 \cdot \nabla \left(\frac{\delta \mathbf{B}_\perp^2}{2\mu} \right) = \mp \Delta \alpha^2 \mu \rho_0 \alpha \mathbf{B}_0 \cdot \nabla P_k. \quad (45)$$

We have previously (Eq. 36) used that in the region exterior to the plume we have as value of $\mu \rho_e \Delta \alpha_e^2 = \frac{1-\zeta}{1+\zeta}$. However, to quantify the term in question, we also need the expression in the interior region:

$$\mu \rho_i \Delta \alpha_i^2 = \frac{\zeta - 1}{\zeta + 1}, \quad (46)$$

i.e. it is the opposite of the value in the exterior.

Then we need to average the contributing term over the entire cross-section, as we have done for the uniturbulence term in Subsec. 4.1.1. We need evaluate

$$\mp \left\{ \int_0^R r dr \mu \rho_i \Delta \alpha_i^2 \alpha \mathbf{B}_0 \cdot \nabla P_{ki} + \int_R^{\gamma R} r dr \mu \rho_e \Delta \alpha_e^2 \alpha \mathbf{B}_0 \cdot \nabla P_{ke} \right\}. \quad (47)$$

Using the results of Eq. 36 and 46, we then have

$$\mp \left(\frac{\zeta - 1}{\zeta + 1} \right) \left\{ \int_0^R r dr \alpha \mathbf{B}_0 \cdot \nabla P_{ki} - \int_R^{\gamma R} r dr \alpha \mathbf{B}_0 \cdot \nabla P_{ke} \right\}. \quad (48)$$

Now we use the fact that the field-aligned gradient will be equal for the internal and external pressure in the WKB approximation, so it can be moved out of the integrals. We then are left to calculate

$$\mp \left(\frac{\zeta - 1}{\zeta + 1} \right) \alpha \mathbf{B}_0 \cdot \nabla \left\{ \int_0^R P_{ki} r dr - \int_R^{\gamma R} P_{ke} r dr \right\}. \quad (49)$$

With the aid of the expressions 16 and 17, and utilising Eqs. 43 and 46 in Van Doorselaere et al. (2020a), we obtain

$$\mp \left(\frac{\zeta - 1}{\zeta + 1} \right) \alpha \mathbf{B}_0 \cdot \nabla \left\{ \frac{\Upsilon^2 \pi R^2}{2\omega^2} (\rho_i \omega_{Ai}^2 - \rho_e \omega_{Ae}^2) (1 - f) \right\}. \quad (50)$$

When we take the filling factor to be small (i.e. $f \ll 1$), then the term in the curly brackets is exactly 0.

4.1.3. Evolution equation for cross-sectionally averaged wave energy

Now we have simplified all terms in the energy evolution equation (Eq. 33). We can now gather all the previous terms and their simplified expression to achieve our goal of obtaining an evolution equation for the kink wave energy density. With the expressions 44 and 50, we may write the final equation for the kink wave energy evolution as

$$\frac{\partial \langle W^\pm \rangle}{\partial t} + \nabla \cdot (\mathbf{Q}_0^\mp \langle W^\pm \rangle) + \frac{\langle W^\pm \rangle}{2} \nabla \cdot \mathbf{V} = -\langle W^\pm \rangle^{3/2} \frac{1}{\pi R^2} \frac{1}{\sqrt{\rho_e}} \sqrt{\frac{2}{5}} \frac{\zeta - 1}{2} \frac{1 - f^{5/2}}{(\zeta + 1 - f)^{3/2}}. \quad (51)$$

This equation has inconvenient units to add up with the traditional expression for the Alfvén wave energy density, since $\langle W^\pm \rangle$ has been integrated over the cross-section of the magnetic flux tube. Thus, it is more convenient to once again normalise it to the relevant cross-sectional area $\pi \gamma^2 R^2$. Thus, we follow the procedure of Goossens et al. (2013) to compute the kink wave energy density. We define

$$W_k^\pm = \frac{\langle W^\pm \rangle}{\pi \gamma^2 R^2} \quad (52)$$

as the cross-sectionally averaged energy density of the kink waves, to obtain as evolution equation for the kink wave energy density

$$\frac{\partial W_k^\pm}{\partial t} + \nabla \cdot (\mathbf{Q}_0^\mp W_k^\pm) + \frac{W_k^\pm}{2} \nabla \cdot \mathbf{V} = -\frac{1}{L_{\perp, \text{VD}}} \frac{1}{\sqrt{\rho_e}} (W_k^\pm)^{3/2}, \quad (53)$$

where we have defined the appropriate length for the damping of the waves as

$$L_{\perp, \text{VD}}(R, \zeta, f) = \left(\frac{1}{R \sqrt{f \pi}} \sqrt{\frac{2}{5}} \frac{\zeta - 1}{2} \frac{1 - f^{5/2}}{(\zeta + 1 - f)^{3/2}} \right)^{-1}. \quad (54)$$

One may say that the introduction of such a length is not any better than the infamous L_{\perp} parameter for the turbulent damping of Alfvén waves. However, the difference is that the Alfvén turbulence parameter is solely based on a phenomenological approach, but here we offer a full description of it for uniturbulence heating. Given that R , f , and ζ all vary with distance along a magnetic field line, it is clear that also $L_{\perp,VD}$ will vary with height in the atmosphere. A reasonable prescription for this parameter may be obtained from initial atmospheric models (e.g. Sishla et al. 2022). In the atmospheric model we use in Sec. 6, the value ranges from 6.3Mm-7.3Mm, which is similar to values for Alfvén waves (e.g. Sharma & Morton 2023, and references therein).

As an alternative, one may consider the theory of Hillier et al. (2019) to quantify the energy cascade rate in the saturated regime. In that case, a new expression would emerge, but it would come down to replacing $L_{\perp,Hillier}$ in the previous equation.

To Eq. 33 an ad-hoc reflection term should be added. We name these terms $\mathcal{R}_{A,k}$ for the respective waves. One could take the same reflection as in van der Holst et al. (2014) for the Alfvén and kink waves alike. Or we may consider the reflection expression from Réville et al. (2020). One could also opt for taking a different reflection of the Alfvén and kink waves.

5. Energy equations for the background

Now we need to incorporate the kink wave energy evolution equation (Eq. 53) into the larger system of AWSOM equations. For this, we need to model the slow background variation through regular MHD, but we supplement the momentum equation with the forces exerted by the wave pressures P_k and P_A . To express the conservation of energy, we need to compute the equation for the conservation of wave energy. To that end, we sum Eq. 33 for the upward and downward Alfvén wave, and Eq. 53 for the upward and downward kink wave. Once again following van der Holst et al. (2014), we also take $CC = 0$. We obtain

$$\begin{aligned} \frac{\partial}{\partial t}(W_A^+ + W_A^- + W_k^+ + W_k^-) + \nabla \cdot (\mathbf{Z}_0^- W_A^+ + \mathbf{Z}_0^+ W_A^- + \mathbf{Q}_0^- W_k^+ + \mathbf{Q}_0^+ W_k^-) + \frac{1}{2}(W_A^+ + W_A^- + W_k^+ + W_k^-) \nabla \cdot \mathbf{V}_0 = \\ - \Gamma^+ W_A^+ - \Gamma^- W_A^- - \frac{1}{L_{\perp,VD}} \frac{1}{\sqrt{\rho_e}} ((W_k^+)^{3/2} + (W_k^-)^{3/2}), \end{aligned} \quad (55)$$

where $\mathbf{Z}_0^{\pm} = \mathbf{V}_0 \pm \mathbf{V}_A$ for the Alfvén waves and \mathbf{Q}_0^{\pm} is the kink phase speed in the moving frame. The term containing the uniturbulent damping is redefined to have the cross-sectionally averaged wave energy density. The terms with Γ^{\pm} are the terms of the Alfvén wave turbulence (van der Holst et al. 2014) containing the infamous L_{\perp} parameter. These terms originate in the $\nabla \cdot \delta \mathbf{Q}_{\perp}^{\mp} W^{\pm}$ terms of Eq. 33 that express the cascade due to interaction with counterpropagating waves. For now, we have assumed that counterpropagating kink waves do not interact (and thus that the corresponding Γ terms are 0). Indeed, it is likely that the cascade due to their interaction is much smaller than the uniturbulent self-cascade (Eq. 53). The last term will be combined with the terms for the work of the wave pressure forces, using the expression in van der Holst et al. (2014):

$$P_A = \frac{W_A^+ + W_A^-}{2}, \quad \text{and} \quad P_k = \frac{W_k^+ + W_k^-}{2\mu\rho_0\alpha^2}. \quad (56)$$

The terms in the right-hand side of Eq. 55 should not be taken into account into the integrated energy equation of MHD plus the waves. Indeed, the cascade energy (be it via Alfvén wave turbulence or uniturbulence) is added into the system as heat. Thus, those damping terms would cancel out with the heating terms.

We have also taken all cross-interactions to be zero. For instance terms like $\delta \mathbf{Z}^+ \cdot \nabla W_k^+$. We could make some Fourier based arguments why these will not contribute, but Guo et al. (2019) have already shown that the presence of Alfvén waves does in fact facilitate the cascade of (admittedly standing) kink waves.

Let us now formulate the conservation equations for the entire system. We start with the conservation of mass and the induction equation:

$$\frac{\partial \rho_0}{\partial t} + \nabla \cdot (\rho_0 \mathbf{V}) = 0, \quad (57)$$

$$\frac{\partial \mathbf{B}_0}{\partial t} - \nabla \times (\mathbf{V} \times \mathbf{B}_0) = 0, \quad (58)$$

which are unchanged from straight MHD. Then, we formulate the conservation of momentum

$$\frac{\partial \rho_0 \mathbf{V}}{\partial t} + \nabla \cdot (\rho_0 \mathbf{V} \mathbf{V} - \frac{1}{\mu} \mathbf{B}_0 \mathbf{B}_0) + \nabla (p + \frac{B_0^2}{2\mu} + P_A + P_k) = -\rho_0 \mathbf{g}(\mathbf{r}), \quad (59)$$

where additionally to the traditional terms (including the gravity \mathbf{g} , depending on the radial distance from the Sun), we have included the wave pressures P_A and P_k .

As the equation for internal energy, we take

$$\frac{\partial}{\partial t} \frac{p}{\gamma - 1} + \nabla \cdot \frac{p \mathbf{V}}{\gamma - 1} + p \nabla \cdot \mathbf{V} = -\mathcal{L} + \mathcal{H}_{A+k}, \quad (60)$$

where we have incorporated radiative losses \mathcal{L} and the heating $\mathcal{H}_{A+k} = \Gamma^+ W_A^+ + \Gamma^- W_A^- + \frac{1}{L_{\perp,VD}(R,\zeta,f)} \frac{1}{\sqrt{\rho_e}} ((W_k^+)^{3/2} + (W_k^-)^{3/2})$ by the Alfvén and kink waves. To obtain the final energy equation, we add Eq. 55, Eq. 60, \mathbf{V} -Eq. 59 and \mathbf{B} -Eq. 58, resulting in

$$\begin{aligned} \frac{\partial}{\partial t} \left(\rho_0 \frac{V^2}{2} + \frac{p}{\gamma-1} + \frac{B_0^2}{2\mu} + \sum W_{A,k}^{\pm} \right) + \nabla \cdot \left(\left[\rho_0 \frac{V^2}{2} + \frac{p}{\gamma-1} + \frac{B_0^2}{2\mu} \right] \mathbf{V} - \mathbf{B}_0 \frac{\mathbf{V} \cdot \mathbf{B}_0}{\mu} \right) \\ + \nabla \cdot \left(\mathbf{Z}_0^- W_A^+ + \mathbf{Z}_0^+ W_A^- + \mathbf{Q}_0^- W_k^+ + \mathbf{Q}_0^+ W_k^- \right) + \nabla \cdot ([P_A + P_k] \mathbf{V}) + (\mu\rho_0\alpha^2 - 1)P_k \nabla \cdot \mathbf{V} = -\mathcal{L} - \rho_0 \mathbf{V} \cdot \mathbf{g}(\mathbf{r}) \end{aligned} \quad (61)$$

where we have used the shorthand $\sum W_{A,k}^{\pm} = W_A^+ + W_A^- + W_k^+ + W_k^-$. Moreover, we have used the expression for P_k in terms of the Q -densities:

$$P_k = \frac{\delta B^2}{2\mu} = \frac{1}{\mu\rho_0\alpha^2} \frac{W_k^+ + W_k^-}{2} = \frac{1+\zeta}{4} (W_k^+ + W_k^-), \quad (62)$$

in the case that $CC = 0$. The factor $(\mu\rho_0\alpha^2 - 1)$ is present in this equation, because of the non-coincidence between the wave pressure P_k and the average of the wave energies. It reduces to $\frac{1-\zeta}{1+\zeta}$ for kink waves. For an Alfvén wave, this term reduces to 0, because the factor $(\mu\rho_0\alpha^2 - 1)$ is zero when $\alpha^2 = 1/\mu\rho_0$, i.e. for an Alfvén wave. The resulting extra term contains the density contrast, which is varying with height in the solar atmosphere. Thus, also here, a model parameter will appear in the equations which needs to be fixed ad-hoc, just like $L_{\perp,VD}$.

Finally, the full set of equations can be written as

$$\frac{\partial \rho_0}{\partial t} + \nabla \cdot (\rho_0 \mathbf{V}) = 0, \quad (63)$$

$$\frac{\partial \mathbf{B}_0}{\partial t} - \nabla \times (\mathbf{V} \times \mathbf{B}_0) = 0, \quad (64)$$

$$\frac{\partial \rho_0 \mathbf{V}}{\partial t} + \nabla \cdot (\rho_0 \mathbf{V} \mathbf{V} - \frac{1}{\mu} \mathbf{B}_0 \mathbf{B}_0) + \nabla \cdot (p + \frac{B_0^2}{2\mu} + P_A + P_k) = -\rho_0 \mathbf{g}(\mathbf{r}), \quad (65)$$

$$\begin{aligned} \frac{\partial}{\partial t} \left(\rho_0 \frac{V^2}{2} + \frac{p}{\gamma-1} + \frac{B_0^2}{2\mu} + \sum W_{A,k}^{\pm} \right) + \nabla \cdot \left(\left[\rho_0 \frac{V^2}{2} + \frac{p}{\gamma-1} + \frac{B_0^2}{2\mu} \right] \mathbf{V} - \mathbf{B}_0 \frac{\mathbf{V} \cdot \mathbf{B}_0}{\mu} \right) \\ + \nabla \cdot \left(\mathbf{Z}_0^- W_A^+ + \mathbf{Z}_0^+ W_A^- + \mathbf{Q}_0^- W_k^+ + \mathbf{Q}_0^+ W_k^- \right) + \nabla \cdot ([P_A + P_k] \mathbf{V}) = -\mathcal{L} - \rho_0 \mathbf{V} \cdot \mathbf{g}(\mathbf{r}) + \frac{\zeta-1}{\zeta+1} P_k \nabla \cdot \mathbf{V}, \end{aligned} \quad (66)$$

$$\frac{\partial W_A^{\pm}}{\partial t} + \nabla \cdot (\mathbf{Z}_0^{\mp} W_A^{\pm}) + \frac{W_A^{\pm}}{2} \nabla \cdot \mathbf{V} = -\Gamma^{\mp} W_A^{\pm} \mp \mathcal{R}_A, \quad (67)$$

$$\frac{\partial W_k^{\pm}}{\partial t} + \nabla \cdot (\mathbf{Q}_0^{\mp} W_k^{\pm}) + \frac{W_k^{\pm}}{2} \nabla \cdot \mathbf{V} = -\frac{1}{L_{\perp,VD}} \frac{1}{\sqrt{\rho_e}} (W_k^{\pm})^{3/2} \mp \mathcal{R}_k. \quad (68)$$

In all of these equations, ρ_0 is actually ρ_e . When averaging the density over a cross-section, we have

$$\frac{1}{\pi\gamma^2 R^2} \int d\phi \int_0^{\gamma R} \rho r dr = \frac{1}{\pi\gamma^2 R^2} (\pi R^2 \rho_i + \pi(\gamma^2 R^2 - R^2) \rho_e) = f\rho_i + (1-f)\rho_e = \rho_e + f(\rho_i - \rho_e).$$

This averaging over the cross-section of the density would occur in the continuity equation and the non-wave pressure terms of the momentum equation. This understanding that the modelled density ρ_0 is really the external density ρ_e has no impact on the modelling that is performed (see next section). However, appropriate values must be taken. Moreover, additional care is needed when implementing radiative losses, or doing forward modelling, both of which are non-linearly weighed with the density.

In Eqs. 67-68 we have included ad-hoc reflection terms. It is important that these reflection terms adhere to the basic principles of conservation of energy: what is taken out of the $+$ -equation must be injected as a source term in the $-$ -equation, and vice versa. Several expressions for the reflection of Alfvén waves exist in the literature (e.g. van der Holst et al. 2014; Downs et al. 2016; Réville et al. 2020). It is less clear what the reflection term for kink waves might be. Surely, it must be proportional to the strength of the longitudinal kink speed gradient. Inspiration for this aspect may be found also in the existence of a cut-off period for kink waves (Pelouze et al. 2023).

After a lot of calculations, it seems that the evolution equation for Alfvén and kink waves (Eq. 67 and Eq. 68 respectively) are eerily similar. However, there is a key difference. On the one hand, the damping term for the Alfvén waves is dependent on the amplitude of the counterpropagating wave (as has been known for a long time, at least in the homogeneous or WKB picture, while in a stratified plasma, the Alfvén waves also acquire a mixed character enabling cascade Velli et al. 1989; Verdini et al. 2009). Thus, upward-propagating Alfvén waves in plumes are hardly damping in the low solar atmosphere because insufficient reflected waves have been generated. On the other hand, the damping term for the kink wave due to uniturbulence only depends on the amplitude of the kink wave itself (and not on its counterpropagating wave). Thus, the damping is at work, even if no counterpropagating waves are generated yet. This is of particular importance in the low part of the solar atmosphere. There the kink waves damp immediately and significantly (damping lengths that are between 0.25 and $10\times$ their wavelengths, i.e. 25Mm-4000Mm, Van Doorselaere et al. 2020a), providing a crucial ingredient in kick-starting the solar wind and coronal heating low down. We thus expect to have a major

contribution of the kink wave heating in the low corona, whereas the traditional Alfvén wave heating takes over higher up (say around $1R_{\odot}$).

A limitation to these wave equations (for the Alfvén wave as well as the kink wave) is that it has been derived for in the WKB limit. We (but also previous authors van der Holst et al. 2014; Réville et al. 2020) have thus used the implicit assumption that the background variables are only slowly varying along the magnetic field. This allows the waves to be described by only a single Elsässer or Q -variable, and decouples the wave modes. However, if the stratification is significant, the waves are modified and will have a mixed character (Velli et al. 1989; Verdini et al. 2009). Thus, the full, true evolution equations will be much more complicated and retain their 3D nature (Zank et al. 2012).

6. Numerical implementation

To show a first proof-of-concept, we have implemented the UAWSOM equations (Eqs. 63-68) in 1D in python using the *fipy* package¹ (Guyer et al. 2009). However, for this proof-of-concept, we have neglected the Alfvén wave equation (Eq. 67, corresponding to taking $W_{\text{A}}^{\pm} \equiv 0$ in the entire simulation). For ease of implementation, we use the equation for internal energy (Eq. 60) instead of Eq. 66. In 1D, the system of equations (Eqs. 63-68) is reduced to a coupled set of 5 differential equations, since the velocity only has a component along z and the induction equation is reduced to $B(z)$ constant (as a function of time). The resulting python implementation serves as a reference implementation for the UAWSOM concept, and has been made available on Gitlab². In this paper, we have used revision 95111d80. In order to check if the wave propagation equations are correctly implemented, we have also performed a simplified test in a stationary background. The python script for that test is also accessible through the Gitlab repository.

In the equations (Eqs. 63-68), we have incorporated the radiative losses, by using the implementation of Hermans & Keppens (2021) of the coronal cooling curve of Dere et al. (2009). We interpolate the cooling curve's tabulated points with a cubic spline to the temperatures needed in the simulation. On top of the terms included in the energy equation above (Eq. 60), we have also incorporated a thermal conduction term as part of its RHS:

$$\text{Thermal conduction} = -\nabla \cdot (\kappa \nabla T), \quad (69)$$

with $\kappa = \kappa_0 T^{5/2}$ and $\kappa_0 = 8 \cdot 10^{-7} \text{erg/cm/s/K}^{7/2}$. In this first implementation, we have neglected the reflection terms $\mathcal{R}_{\text{k}} = 0$ in the equation for the kink wave energy (Eq. 68). The correct values are not known (Pelouze et al. 2023) and should be investigated in a separate modelling paper. Gravity is fixed at $\mathbf{g}(z) = 274 \text{m/s}^2 \mathbf{1}_z$.

The python programme has as option to read in an *numpy* savefile for its initial condition. However, here we show some results from its start of a pre-implemented plasma configuration. In that pre-implemented configuration, we use as equilibrium

$$\rho(z) = \rho_0 \exp(-z/H), \quad (70)$$

$$V(z) = 0, \quad (71)$$

$$B(z) = B_0 \frac{R_{\odot}^2}{(z + R_{\odot})^2}, \quad (72)$$

$$R(z) = R_0 \frac{B_0^2}{B(z)^2}, \quad (73)$$

$$\zeta = (\zeta_0 - 1) \exp\left(-\frac{z}{5R_{\odot}}\right) + 1, \quad (74)$$

with the initial values ρ_0 is taken equivalent to a number density of 10^9cm^{-3} , $H = 50 \text{Mm}$, $B_0 = 20 \text{G}$, $\zeta_0 = 5$, and $R_0 = 1 \text{Mm}$. We fix the initial temperature in the entire domain at $T_0 = 1 \text{MK}$.

The initial conditions for W_{k}^{\pm} are taken as

$$W_{\text{k}}^{-} = W_0 \left(\frac{1}{2} \cos\left(\frac{\pi z}{\delta}\right) + \frac{1}{2} \right), \quad \text{for } z < \delta, \quad (75)$$

$$W_{\text{k}}^{-} = 0, \quad \text{elsewhere,} \quad (76)$$

$$W_{\text{k}}^{+} = 0, \quad (77)$$

with $\delta = 30 \text{Mm}$ and $W_0 = 4 \cdot 10^{-4} \text{J/m}^3$. This smooth initial condition for W_{k}^{-} was chosen so that an initial abrupt start from a non-zero boundary condition would not lead to difficulties with the boundary conditions.

¹ <https://www.ctcms.nist.gov/fipy/>

² https://gitlab.kuleuven.be/plasma-astrophysics/research/tom_s-projects/uawsom.git

As boundary conditions we take the following at the bottom boundary:

$$\frac{d\rho}{dz} = 0, \quad (78)$$

$$V = 0, \quad (79)$$

$$\frac{dE_{\text{th}}}{dz} = \frac{1}{\gamma - 1} \frac{dp}{dz} = -\frac{g\rho}{\gamma - 1}, \quad (80)$$

$$W_{\text{k}}^- = W_0, \quad (81)$$

$$\frac{dW_{\text{k}}^+}{dz} = 0, \quad (82)$$

where the condition for the thermal energy E_{th} expresses a continuous isothermal stratification beyond the computational domain. At the top boundary, we put as boundary conditions

$$\frac{d\rho}{dz} = 0, \quad (83)$$

$$\frac{dV}{dz} = 0, \quad (84)$$

$$\frac{dE_{\text{th}}}{dz} = \frac{1}{\gamma - 1} \frac{dp}{dz} = -\frac{g\rho}{\gamma - 1}, \quad (85)$$

$$\frac{dW_{\text{k}}^-}{dz} = 0, \quad (86)$$

$$W_{\text{k}}^+ = \frac{W_0}{200}. \quad (87)$$

Our aim was to have reasonably open boundary conditions at the top. However, Fig. 3 shows that there are still reflected slow waves in the simulation as can be seen from bouncing flows between the boundaries.

We display the first 55s of runtime (1000 iteration steps with *fpy*) in Fig. 1. The top 6 panels in the figure show the system variables (ρ , V , E_{th} , W_{k}^+) and also the temperature T . The bottom 6 panels show the simulation but with a much lower energy W_{k}^- in the kink wave (by setting the left boundary condition for this variable to $W_0/200$). As visible in the bottom right panel (of the top 6), the kink wave is propagating into the system with the appropriate kink speed. The resulting energy dissipation and deposition is leading to heating, as can be seen by comparing the temperature scale of the T -panel of the top 6 and the bottom 6. The temperature T is gradually decreasing in both, because of the radiative losses. However, the top panel with the kink wave heating has a slightly higher temperature than the non-heated simulation. This is more clearly shown in Fig. 2, where the final temperature profile as a function of height is shown for the top and bottom simulation of Fig. 1, corresponding to the case of “heating” and “no heating”. Additionally, we display the initial temperature of 1MK and also a simulation with kink wave heating, but where the radiative losses have been switched off. The graph in Fig. 2 clearly shows that the wave heating indeed increases the temperature, either above the initial temperature in the case of no radiative losses, or at least above the temperature in a simulation with only just radiative cooling.

The effect of the kink wave pressure P_{k} is also visible in the panels of Fig. 1 showing the velocity V . The top right panel with kink wave pressure shows a gentle upflow, while the bottom panels show a gradual downflow. The latter happens because of the restructuring of the plasma due to the radiative cooling. Also visible in that panel (V of the bottom 6 panels) is the effect of the top boundary, which has a propagating signal associated with the downward kink wave, but also a signal propagating with the sound speed.

The effect of the numerical diffusivity is shown in the bottom left panel W_{k}^+ . The front of the W_{k}^+ energy should theoretically remain a sharp interface, but it is clear that during its propagation it is smoothed out.

In Fig. 3, we show the longer duration run of the simulation with the kink wave heating, for 3100s. In the panel with velocity V , it is shown that there is a gradual upflow generated by the kink wave driving, on the order of 5 – 10km/s. However, at times later than 2000s and height above 70Mm, numerical instabilities show up, which eventually crash the simulation. Some additional viscosity terms might damp out the instabilities. Still, the panel clearly shows that upflows are driven by the kink wave pressure, because these upflows are absent in the non-driven simulation.

As can be seen in the temperature panel T , the temperature gradually decreases. However, it does not decrease as much as expected without wave heating. The cooling times in the simulation, calculated as $\tau = E_{\text{th}}/\mathcal{L}$ are between 2700 – 20000s. In the panel, it is clearly visible that the plasma is not cooling down as much as expected from these cooling time scales, given that the temperature’s minimum value is 0.45MK $> T_0/e$. Thus, the kink waves are indeed partially heating the plasma, or at least sustaining it against radiative losses (similar to Shi et al. 2021).

The cooling by the radiative losses is not entirely counteracted, and this is shown by the strong decrease of the initial temperature. As a result of the steady cooling, the plasma is restructuring to fit with the new quasi-equilibrium. That leads to a drainage of density towards the footpoint, as is visible in the top left panel.

It is clear that this simulation is not the final simulation needed for concluding the UAWSOM model and determining its usefulness. Further work is needed, particularly for varying equilibrium parameters and driving parameters. It was not our aim to obtain a steady solution for the solar atmosphere, but rather a proof-of-concept for the application of the UAWSOM equations (Eqs. 63-68).

7. Conclusions

In this paper, we have employed the formalism of Q -variables. This formalism gives equations co-propagating with a specific wave. We have used the equations of Van Doorselaere et al. (2024) and recast the equations to an energy propagation equation. We have found that all waves show self-damping through non-linear effects, except for Alfvén waves. This is visible in the energy equation (Eq. 33) because of terms proportional to $\Delta\alpha^2$, a parameter which is always non-zero except for Alfvén waves.

We have further specialised the energy propagation equation to the case of kink waves. To that end, we have followed the approach of Van Doorselaere et al. (2020a) and averaged out the wave energy equation over the cross-section of the plume. From that averaging process, we have found a single equation for kink wave energy evolution (Eq. 53). This equation introduced the $L_{\perp, \text{VD}}$ factor, but unlike Alfvén wave turbulence this parameter is given in terms of background properties. We have found that the energy dissipation term is proportional to $(W_{\text{k}}^{\pm})^{3/2}$.

Such a proportionality of the damping term was also previously proposed by Zank et al. (1996). However, in his case, the damping term was multiplied with the $f(\sigma_c)$ (which becomes zero if cross-helicity $\sigma_c = \pm 1$, i.e. only one of the counterpropagating waves). Here, on the other hand, the $f(\sigma_c)$ remains non-zero even if only one of the propagation directions is present. Such a case was observationally considered by Adhikari et al. (2023). The presence of this term in the equation shows that kink waves (or any other wave, except for Alfvén waves) will damp even if a wave is propagating in only one direction occurs.

Subsequently, we have combined the energy propagation equation for kink waves (Eq. 53), with a slowly varying (in the WKB sense) background that is governed by the MHD equations. The resulting system (Eqs. 63-68, which we have dubbed the UAWSOM system) has the traditional conservation of mass, momentum and energy, but is supplemented by wave energy equations. The latter wave energy equations keep track of the wave energy and the wave's damping. The wave energy is then added to the total energy and incorporated in the energy conservation equation. This ensures that energy loss of the wave results in the increase of thermal energy and thus heating of the plasma.

For now, we have considered this system of equations to be an extension to the classical AWSOM model of van der Holst et al. (2014). On top of the AWSOM model, we have additionally incorporated the kink wave driving. The kink wave evolution equation is apparently very similar to the Alfvén wave evolution equation. However, the difference is in the damping term. The Alfvén waves require counterpropagating waves to initiate the cascade to turbulent heating and low in the atmosphere the reflected waves are not strong enough to generate sufficient heating. The damping term for the kink waves, however, is also operating when there is no counterpropagating wave. Thus, the kink waves can already start heating the plasma low down in the atmosphere where the damping is further enhanced by the large density gradients of the flux tubes (and despite the absence of reflected waves). It may thus well be that kink waves play a key role in providing the jump start to solar coronal and solar wind heating low down in (say) the first few 100Mm.

In principle, the formalism for the addition of a kink wave equation can also be used to incorporate a 3rd equation on the slow wave driving and development. That would allow us to model the interaction of the parametric instability and its influence on the reflection of the Alfvén waves. Then, we would be able to capture the essential physics in the Shoda et al. (2019) paper in a similar 1D model. This is left for a future work.

Lastly, we have implemented the UAWSOM equations in a python module, where we considered the 1D version of the full set of equations (Eqs. 63-68, albeit with Alfvén wave power set to 0). We have shown that the kink wave driving of the solar atmosphere leads to the generation of upflows. Moreover, the uniturbulent damping of the kink waves leads to the heating of the plasma, which seems most significant in the low corona. In some regions in our simulation, the kink wave heating could sustain the plasma against the cooling by radiative losses, but in others it could not. These initial results with the python implementation show that further work is needed, but it also showcases the potential that the UAWSOM model holds. As such, the implementation offered in this article serves as a proof-of-concept rather than a full investigation of this model's usefulness.

As future work, we will compare 1D but also 3D solar atmospheres which are driven solely by Alfvén waves, solely by kink waves and mixed models (with varying ratios of kink and Alfvén wave energy content). The comparison of these models to observations will allow us to place bounds on the ratio of kink wave and Alfvén wave driving energy.

Acknowledgements. TVD was supported by the European Research Council (ERC) under the European Union's Horizon 2020 research and innovation programme (grant agreement No 724326), the C1 grant TRACESpace of Internal Funds KU Leuven, and a Senior Research Project (G088021N) of the FWO Vlaanderen. Furthermore, TVD received financial support from the Flemish Government under the long-term structural Methusalem funding program, project SOUL: Stellar evolution in full glory, grant METH/24/012 at KU Leuven. The research that led to these results was subsidised by the Belgian Federal Science Policy Office through the contract B2/223/P1/CLOSE-UP. It is also part of the DynaSun project and has thus received funding under the Horizon Europe programme of the European Union under grant agreement (no. 101131534). Views and opinions expressed are however those of the author(s) only and do not necessarily reflect those of the European Union and therefore the European Union cannot be held responsible for them. TVD is grateful for the hospitality of Iñigo Arregui (IAC, Tenerife) where these results were discussed.

NM acknowledges Research Foundation – Flanders (FWO Vlaanderen) for their support through a Postdoctoral Fellowship.

MVS acknowledges support from the French Research Agency grant ANR STORMGENESIS #ANR-22-CE31-0013-01.

This research was supported by the International Space Science Institute (ISSI) in Bern, through ISSI International Team project #560.

References

- Adhikari, L., Zank, G. P., Telloni, D., Zhao, L. L., & Pitna, A. 2023, in *Journal of Physics Conference Series*, Vol. 2544, *Journal of Physics Conference Series (IOP)*, 012007
- Alvarado-Gómez, J. D., Cohen, O., Drake, J. J., et al. 2022, *ApJ*, 928, 147
- Anfinogentov, S., Nakariakov, V. M., Mathioudakis, M., Van Doorselaere, T., & Kowalski, A. F. 2013, *ApJ*, 773, 156
- Anfinogentov, S. A., Nakariakov, V. M., & Nisticò, G. 2015, *A&A*, 583, A136
- Antolin, P. & Van Doorselaere, T. 2019, *Frontiers in Physics*, 7, 85
- Banerjee, D., Teriaca, L., Doyle, J. G., & Wilhelm, K. 1998, *A&A*, 339, 208

- Bruno, R. & Carbone, V. 2013, *Living Reviews in Solar Physics*, 10, 2
- Cohen, O., Glocer, A., Garraffo, C., et al. 2024, *ApJ*, 962, 157
- De Moortel, I. & Howson, T. A. 2022, *ApJ*, 941, 85
- De Pontieu, B., Carlsson, M., Rouppe van der Voort, L. H. M., et al. 2012, *ApJ*, 752, L12
- Dere, K. P., Landi, E., Young, P. R., et al. 2009, *A&A*, 498, 915
- Downs, C., Lionello, R., Mikić, Z., Linker, J. A., & Velli, M. 2016, *ApJ*, 832, 180
- Evans, R. M., Opher, M., Oran, R., et al. 2012, *ApJ*, 756, 155
- Evensberget, D. & Vidotto, A. A. 2024, *MNRAS*, 529, L140
- Gao, Y., Tian, H., Van Doorselaere, T., & Chen, Y. 2022, *ApJ*, 930, 55
- Goossens, M., Andries, J., Soler, R., et al. 2012, *ApJ*, 753, 111
- Goossens, M., Hollweg, J. V., & Sakurai, T. 1992, *Sol. Phys.*, 138, 233
- Goossens, M., Terradas, J., Andries, J., Arregui, I., & Ballester, J. L. 2009, *A&A*, 503, 213
- Goossens, M., Van Doorselaere, T., Soler, R., & Verth, G. 2013, *ApJ*, 768, 191
- Guo, M., Van Doorselaere, T., Karpelas, K., et al. 2019, *ApJ*, 870, 55
- Guyer, J. E., Wheeler, D., & Warren, J. A. 2009, *Computing in Science and Engineering*, 11, 6
- Hahn, M. & Savin, D. W. 2013, *ApJ*, 776, 78
- Hermans, J. & Keppens, R. 2021, *A&A*, 655, A36
- Hillier, A., Barker, A., Arregui, I., & Latter, H. 2019, *MNRAS*, 482, 1143
- Ismayilli, R., Van Doorselaere, T., Goossens, M., & Magyar, N. 2022, *Frontiers in Astronomy and Space Sciences*, 8, 241
- Ismayilli, R., Van Doorselaere, T., Magyar, N., Changmai, M., & Verdini, A. 2024, *Physics of Fluids*, 36, 065109
- Karpelas, K. & Van Doorselaere, T. 2018, *A&A*, 610, L9
- Karpelas, K. & Van Doorselaere, T. 2021, *ApJ*, 908, L7
- Lim, D., Van Doorselaere, T., Berghmans, D., et al. 2023, *ApJ*, 952, L15
- Magyar, N. & Nakariakov, V. M. 2021, *ApJ*, 907, 55
- Magyar, N., Van Doorselaere, T., & Goossens, M. 2017, *Nat. Sci. Rep.*, 7
- Magyar, N., Van Doorselaere, T., & Goossens, M. 2019, *ApJ*, 882, 50
- Morton, R. J., Tiwari, A. K., Van Doorselaere, T., & McLaughlin, J. A. 2021, *ApJ*, 923, 225
- Nakariakov, V. M., Zhong, S., Kolotkov, D. Y., et al. 2024, *Reviews of Modern Plasma Physics*, 8, 19
- Nechaeva, A., Zimovets, I. V., Nakariakov, V. M., & Goddard, C. R. 2019, *ApJS*, 241, 31
- Nisticò, G., Nakariakov, V. M., & Verwichte, E. 2013, *A&A*, 552, A57
- Pant, V. & Van Doorselaere, T. 2020, *ApJ*, 899, 1
- Parashar, T. N., Goldstein, M. L., Maruca, B. A., et al. 2020, *ApJS*, 246, 58
- Pelouze, G., Van Doorselaere, T., Karpelas, K., Riedl, J. M., & Duckenfield, T. 2023, *A&A*, 672, A105
- Petrova, E., Magyar, N., Van Doorselaere, T., & Berghmans, D. 2023, *ApJ*, 946, 36
- Petrova, E., Van Doorselaere, T., Berghmans, D., et al. 2024, *arXiv e-prints*, arXiv:2404.10577
- Réville, V., Velli, M., Panasenco, O., et al. 2020, *ApJS*, 246, 24
- Riley, P., Downs, C., Linker, J. A., et al. 2019, *ApJ*, 874, L15
- Sharma, R. & Morton, R. J. 2023, *Nature Astronomy*, 7, 1301
- Shetye, J., Verwichte, E., Stangalini, M., & Doyle, J. G. 2021, *ApJ*, 921, 30
- Shi, M., Van Doorselaere, T., Guo, M., et al. 2021, *ApJ*, 908, 233
- Shoda, M., Suzuki, T. K., Asgari-Targhi, M., & Yokoyama, T. 2019, *ApJ*, 880, L2
- Shrivastav, A. K., Pant, V., Berghmans, D., et al. 2023, *arXiv e-prints*, arXiv:2304.13554
- Sishtla, C. P., Pomoell, J., Kilpua, E., et al. 2022, *A&A*, 661, A58
- Suzuki, T. K. & Inutsuka, S.-i. 2005, *ApJ*, 632, L49
- Terradas, J., Andries, J., Goossens, M., et al. 2008, *ApJ*, 687, L115
- Thurgood, J. O., Morton, R. J., & McLaughlin, J. A. 2014, *ApJ*, 790, L2
- Tian, H., McIntosh, S. W., Wang, T., et al. 2012, *ApJ*, 759, 144
- Tiwari, A. K., Morton, R. J., & McLaughlin, J. A. 2021, *ApJ*, 919, 74
- Tomczyk, S. & McIntosh, S. W. 2009, *ApJ*, 697, 1384
- Tomczyk, S., McIntosh, S. W., Keil, S. L., et al. 2007, *Science*, 317, 1192
- van der Holst, B., Sokolov, I. V., Meng, X., et al. 2014, *ApJ*, 782, 81
- Van Doorselaere, T., Gijsen, S. E., Andries, J., & Verth, G. 2014, *ApJ*, 795, 18
- Van Doorselaere, T., Li, B., Goossens, M., Hnat, B., & Magyar, N. 2020a, *ApJ*, 899, 100
- Van Doorselaere, T., Magyar, N., Sieyra, M. V., & Goossens, M. 2024, *Journal of Plasma Physics*, 90, 905900113
- Van Doorselaere, T., Nakariakov, V. M., & Verwichte, E. 2008, *ApJ*, 676, L73
- Van Doorselaere, T., Srivastava, A. K., Antolin, P., et al. 2020b, *Space Sci. Rev.*, 216, 140
- Velli, M., Grappin, R., & Mangeney, A. 1989, *Physical Review Letters*, 63, 1807
- Verdini, A., Velli, M., & Buchlin, E. 2009, *ApJ*, 700, L39
- Verdini, A., Velli, M., Matthaeus, W. H., Oughton, S., & Dmitruk, P. 2010, *ApJ*, 708, L116
- Wang, T., Ofman, L., Davila, J. M., & Su, Y. 2012, *ApJ*, 751, L27
- Zank, G. P., Dosch, A., Hunana, P., et al. 2012, *ApJ*, 745, 35
- Zank, G. P., Matthaeus, W. H., & Smith, C. W. 1996, *J. Geophys. Res.*, 101, 17093

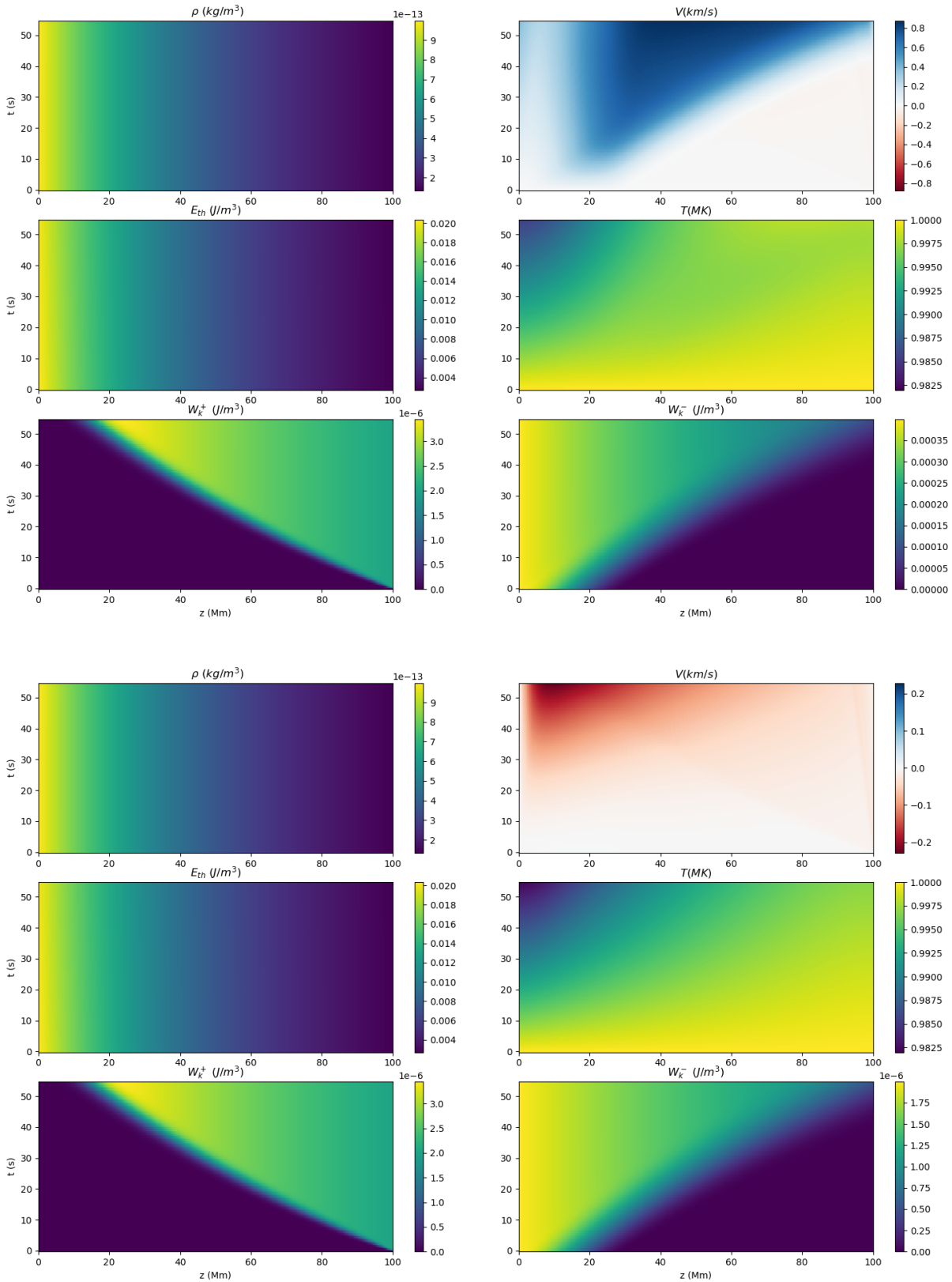


Fig. 1. The first 1000 time steps for the large simulation. Top 6 panels: Simulation variables for the simulation with wave heating. As in the following figures, the 6 panels consist of density ρ , velocity V , thermal energy E_{th} , temperature T and wave energies W_k^\pm . Bottom 6 panels: The same, but with a much lower influx value of $W_k^- = W_0/200$ at the left boundary, resulting in almost no kink wave heating.

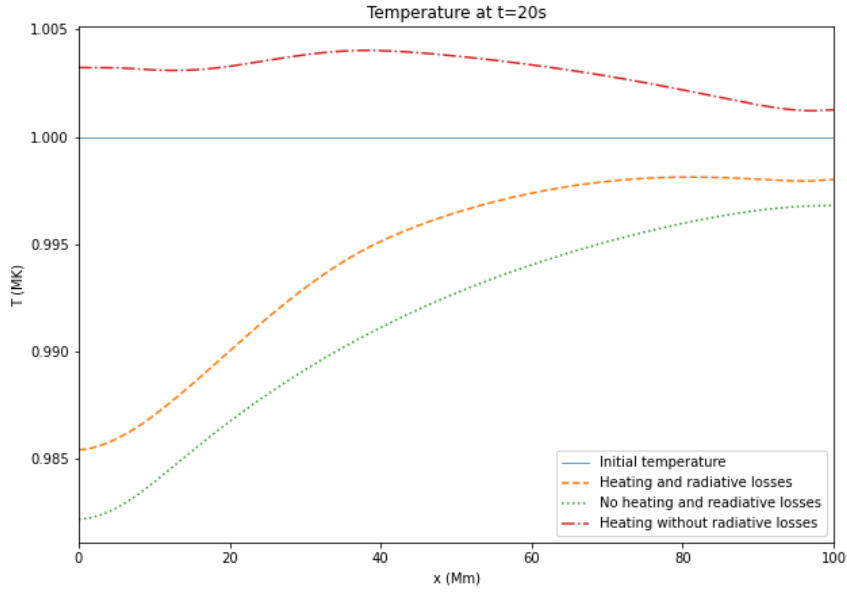


Fig. 2. The temperature profile as a function of height at the end of the short simulations shown in Fig. 1, for 3 different simulations: one with kink wave heating and no radiative losses, one with kink wave heating and radiative losses, and one without kink wave heating and radiative losses.

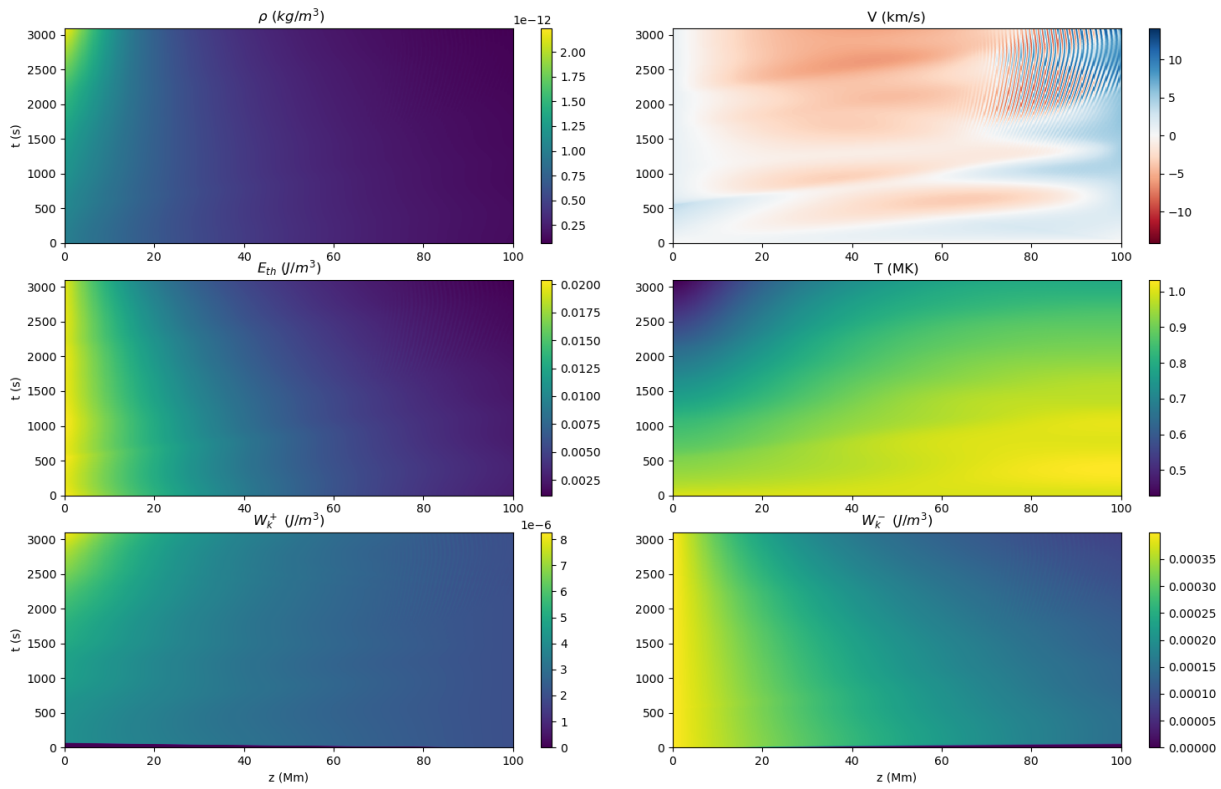


Fig. 3. The continuation of the simulation with kink wave heating and radiative losses until a time of 3100s.

Appendix A: Relation between wave energy w and Q -density W

We have previously introduced the wave energy density in Eq. 13, which we repeat here for convenience:

$$w^\pm = \frac{\rho_0(\delta\mathbf{Z}^\pm)^2}{4}.$$

We had also introduced the Q -density W^\pm in Eq. 28:

$$W^\pm = \frac{\rho_0}{4} (\delta\mathbf{Q}_\perp^\pm)^2.$$

These two expressions apparently do not coincide. In this section, we explore the interrelation between these two expressions. To calculate the Q -density, we start from Eqs. 7-11 to obtain

$$\delta Q_r^\pm = \frac{\partial \mathcal{R}}{\partial r} \frac{\Omega \mp \alpha k_z B_0}{\rho_0(\Omega^2 - \omega_A^2)} \cos \varphi \sin(k_z z - \omega t), \quad (\text{A.1})$$

$$\delta Q_\varphi^\pm = -\frac{\mathcal{R}}{r} \frac{\Omega \mp \alpha k_z B_0}{\rho_0(\Omega^2 - \omega_A^2)} \sin \varphi \sin(k_z z - \omega t). \quad (\text{A.2})$$

As discussed in Van Doorselaere et al. (2024), we compute α in order to describe the wave in the co-moving waveframe. Thus, we have that

$$\Omega = \mp \alpha k_z B_0. \quad (\text{A.3})$$

We thus find that (for example) the positive, downward wave energy is

$$W^+ = \frac{\Omega^2}{\rho_0(\Omega^2 - \omega_A^2)^2} \left(\left(\frac{\partial \mathcal{R}}{\partial r} \right)^2 \cos^2 \varphi + \left(\frac{\mathcal{R}}{r} \right)^2 \sin^2 \varphi \right) \sin^2(k_z z - \omega t) \quad (\text{A.4})$$

and $W^- = 0$. Indeed, the downward propagating wave is solely described by $\delta\mathbf{Q}_\perp^+$. Now, we take the cross-sectional and wavelength average of the Q -density $\langle W^\pm \rangle$, where the radial integral is taken for the volume ($r \in [0, \gamma R]$) in which this plume is the dominant structure (Van Doorselaere et al. 2014). We relate this outer boundary γR to the filling factor f of the corona through the relation of Van Doorselaere et al. (2014)

$$\gamma^2 = \frac{1}{f}. \quad (\text{A.5})$$

Using a similar procedure as Van Doorselaere et al. (2014) and Van Doorselaere et al. (2024), we have as cross-sectionally averaged Q -density $\langle W^\pm \rangle$ (see Eq. 43):

$$\langle W^\pm \rangle = \pi A^2 \Omega^2 \int_0^R \frac{r dr}{R^2 \rho_i(\Omega^2 - \omega_{Ai}^2)^2} + \int_R^{\gamma R} \frac{R^2 r dr}{r^4 \rho_e(\Omega^2 - \omega_{Ae}^2)^2}, \quad (\text{A.6})$$

$$= \frac{\pi A^2 \Omega^2}{2} \frac{1}{\rho_e^2(\Omega^2 - \omega_{Ae}^2)^2} (\rho_i + \rho_e(1 - f)), \quad (\text{A.7})$$

$$= \pi R^2 \Upsilon^2 \frac{\rho_i + \rho_e(1 - f)}{2}. \quad (\text{A.8})$$

In the second line, we have used the dispersion relation for the kink wave with $\rho_i(\Omega^2 - \omega_{Ai}^2) = \rho_e(\Omega^2 - \omega_{Ae}^2)$, and in the third line we have used the expression for the wave amplitude Υ (see Eq. 5). The term without f corresponds exactly to the expression of the energy density $\langle w \rangle$ (see e.g. Eq. 10 in Van Doorselaere et al. 2014). There is only a difference in the term proportional to the filling factor f . Note that if there are no other structures in the corona, we would integrate until $r \rightarrow \infty$ and consequently $f = 0$, and hence the expression of the energy density $\langle w \rangle$ is in that case the same as $\langle W^\pm \rangle$.

To explain this (seemingly remarkable) coincidence between the expressions for $\langle W^\pm \rangle$ and $\langle w \rangle$, we start again from the expression for the wave energy density w (see Eq. 13) and the Q -density (Eq. 28).

$$W^\pm = \frac{\rho_0}{4} (\delta\mathbf{V}_\perp \pm \alpha \delta\mathbf{B}_\perp)^2 = \frac{\rho_0}{4} (\delta V_\perp^2 + \alpha^2 \delta B_\perp^2 \pm 2\alpha \delta\mathbf{B}_\perp \cdot \delta\mathbf{V}_\perp), \quad (\text{A.9})$$

$$w = w^+ + w^- = \frac{\rho_0}{2} (\delta V_\perp^2 + \frac{\delta B_\perp^2}{\mu \rho_0}). \quad (\text{A.10})$$

The equations are seemingly different, but this difference is only apparent indeed. By construction, we have that

$$\delta\mathbf{Q}_\perp^\mp = 0 \quad (\text{A.11})$$

for the oppositely propagating wave. Thus, we must have

$$\delta\mathbf{V}_\perp \mp \alpha \delta\mathbf{B}_\perp = 0, \quad \text{or} \quad \delta\mathbf{V}_\perp = \pm \alpha \delta\mathbf{B}_\perp. \quad (\text{A.12})$$

Then, we see that the Q -density equals

$$W^{\pm} = \rho_0 \delta V_{\perp}^2. \quad (\text{A.13})$$

This is equal to the wave energy w in case of equipartition of the wave (over the domain in which the wave energy is averaged). Thus, for well-behaved waves (such as the kink wave, which has equipartition, Goossens et al. 2013), the Q -density is exactly equal to the wave energy density. As explained in Goossens et al. (2013), the equipartition between magnetic and kinetic energy for kink waves is only satisfied when considering the entire domain. Here however, the spatial domain is limited to a distance γR , so that the equipartition is not exact, explicit by the presence of the term containing the filling factor f .